Gas Phase Spectroscopy

(BL2B2, 3A1, 3A2, 4B, 8A1)

(FEL & BL3A1 & BL7B)

The investigation of excited states of Xe dimers by synchronization of FEL and SR Pulses at UVSOR

Tatsuo GEJO, Eiji SHIGEMASA, Eiken NAKAMURA, Masahito HOSAKA, Shigeru KODA, Akira MOCHIHASHI, Masahiro KATOH, Jun-ichiro YAMAZAKI, Kenji HAYASHI, Yoshifumi TAKASHIMA and Hiroyuki HAMA[a]

Institute for Molecular Science, Myodaiji, Okazaki 444-8585, Japan

[a]*Laboratory of Nuclear Science, Tohoku University, Sendai 980 Japan*

Introduction

Storage Ring Free Electron Laser (SRFEL or FEL) has been developed at many synchrotron radiation (SR) facilities all over the world as a powerful light source owing to its high power, high coherence and unique temporal feature. Pump and probe experiments using FEL and SR pulses have been tried to perform for the last decade, since the FEL pulse naturally synchronizes with the SR one. Recently, we have successfully carried out the two-photon double-resonant excitation on Xe atoms, utilizing a SR pulse as a pump and an FEL pulse as a probe light. Here we report the results on the pressure-dependent measurements that were applied to the same system.

Experiments

In the present work, separate experiments were implemented at two different beamlines of BL3A1 and BL7B at UVSOR. At BL3A1, no monochromator is installed. Therefore, an LiF filter was employed to suppress higher order harmonics of the undulator radiation. The FEL pulses were extracted through the backward mirror of the optical klystron at BL5 and transported to experimental stations through series of multi-layer mirrors. The flight path of FEL, which was adjusted to synchronize timing between the FEL and the SR pulses, was about 30 m. A focusing mirror (f = 10 m) was placed in the center of the flight path to keep the beam size of FEL small throughout the transport. About 69 % of the extracted power was transferred to the experimental station. Fine-tuning of the delay timing was made by using a movable optical delay system (50 cm) at the experimental station. The FEL and SR pulses introduced, coaxially crossed an effusive jet of Xe atoms from a gas nozzle. The singly charged Xe ions produced in the interaction region were detected by means of a conventional channeltron. During the experiment, there were serious background signals due to scattered stray light of SR pulses (typically about 10^5 counts/sec), which made it difficult to detect the real ion signals. In order to overcome such a difficulty, we temporarily employed the Q-switching technique. With use of this technique, much larger peak power of FEL than that in the normal operation is provided, although the duration of lasing becomes relatively short (~ 0.2 msec). However, if events are selected only during this duration, the improvement of signal to noise ratio (S/N) by a factor of 100 can be achieved. A newly developed feedback system was operated to stabilize the lasing throughout the course of the experiments.

Results and discussion

Fig. 1 shows the excitation spectrum near the Xe* $5p^5 5d$ resonance region obtained by setting the FEL wavelength to the maximum of the $5d \rightarrow 4f'$ transition. The background pressure indicated in the figure was kept constant during the measurement. The clear enhancement just below the Xe* $5p^5 5d$ resonance around 117.5 nm is observed in Fig. 1, which has not been detected in the previous measurements at a lower pressure. This result strongly suggests that the newly found structure indicated by the arrow is relevant to the formation of Xe clusters, mainly dimers. The potential energy curves for only three-lowest excited states of Xe_2 have been intensively investigated both experimentally [1] and theoretically [2], but no information about the other excited states is obtainable from the literature. However, from consideration of the excitation energy, it seems to be safe to say that an excited state of Xe_2 exists near the $5p \rightarrow 5d$ transition of the Xe atom, which act as intermediate states in the present experiments. Figs. 2 and 3 represent the ion yield spectra in the vicinity of the autoionization Xe* $5p^5 4f$ resonance state and near the $5p_{1/2}$ ionization threshold, respectively, which were obtained by setting the SR wavelength to the maximum of the $5p \rightarrow 5d$ transition. The structures shown by the arrows, which have never been identified at low-pressure measurements, also imply the existence of the excited state of Xe_2. Further improvement on the total performance of the experimental setup is desired for detailed discussion.

References [1] O. Dutuit et al., J. Chem. Phys. 73 (1980) 3107.

[2] J.B. Nee et al., Chem. Phys. Lett. 318 (2000) 402.

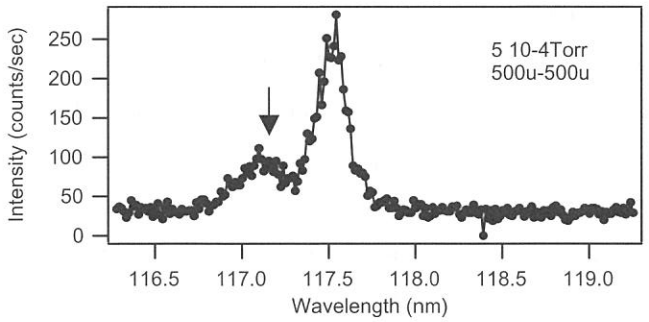

Fig. 1 Two-photon ionization signal of Xe dimers as a function of the wavelength of SR.

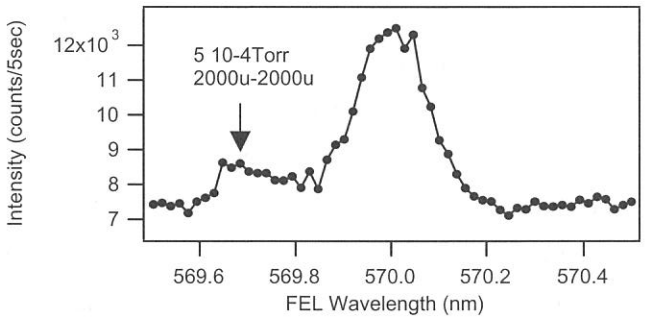

Fig. 2 Two-photon ionization signal of Xe dimers as a function of the wavelength of FEL.

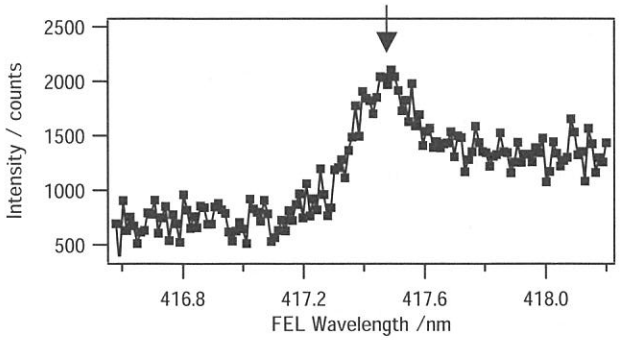

Fig. 3 Two-photon ionization signal of Xe dimers as a function of the wavelength of FEL

(BL2B2)

Molecular- and Atomic-Like Photoionization of C_{60} in the Extreme Ultraviolet

J. Kou,[a] T. Mori,[a] M. Ono[a], Y. Haruyama,[b] Y. Kubozono[a,b], K. Mitsuke[a,c]

[a]*Department of Vacuum UV Photo-Science, The Institute for Molecular Science, Myodaiji, Okazaki 444-8585, Japan*

[b]*Department of Chemistry, Faculty of Science, Okayama University, Okayama 700-8530, Japan*

[c]*Graduate University for Advanced Studies, Myodaiji, Okazaki 444-8585, Japan*

Introduction

Optical response of C_{60} has attracted considerable attention in connection with its characteristic electronic structure originating from the high-symmetrical molecular structure. In 1992, Hertel et al. have observed the strong peak lying at $h\nu$ ~ 20 eV with a FWHM of ~10 eV [1]. They assumed this peak ascribable to a giant plasmon resonance as a collective excitation. Very recently, Colavita et al. have calculated total photoionization cross sections at $h\nu$ = 7.6 – 80 eV [2]. Their spectrum calculated at $h\nu$ = 16 – 50 eV indicates many fine structures which comprise several resonances close to one another. These fine structures are explained to arise from shape resonances. So far there are a limited number of experimental data points above 25 eV. In particular only a single point at 40.8 eV is available between 35 and 283 eV to our knowledge.

In the present study, we tried to obtain reliable and reproducible data of the ion yield from photoionization of C_{60} with relatively good energy resolution [3]. The observed ion signal counts were normalized carefully to both the flux of the C_{60} molecular beam and the photon flux of synchrotron radiation. This experimental setup and elaborate procedure allow us to achieve detailed photoion yield spectra at $h\nu$ > 25 eV and to uncover a general tendency and local features appearing in the valence photoabsorption cross section curve of C_{60}.

Experiments

The detail of the experimental setup will be described elseehere [4]. A monochromatized synchrotron radiation (SR) with linear polarization was provided from an 18 m-length Dragon-type monochromator [5]. The molecular beam of C_{60} was generated by heating C_{60} powder to approximately 450 °C with a resistive heater. The C_{60} beam was irradiated with SR and then photoions were produced in the intersection region. The photoions from C_{60} were analyzed by the use of a TOF mass spectrometer. A photoion yield spectrum of C_{60} was constructed by normalizing the ion counts at each $h\nu$ to the photon flux and molecular-beam intensity monitored at the same time, and by collecting the normalized counts consecutively with changing $h\nu$ at an interval of 0.1 eV.

Results and Discussion

The solid curves in Fig. 1 show the ion yield of C_{60}^+ from C_{60}. Our ion yield at $h\nu$ ~ 23 - 50 eV reflects the molecular character of C_{60} in its valence photoionization. Below 40 eV the baseline of the ion yield curve tends

to decrease with increasing $h\nu$, since this region is situated on the higher energy side of the prominent peak at $h\nu$ ~ 20 eV. Two broad structures are clearly seen at 26 and 34 eV, which will be referred to in the following discussion as peak *A* and *B*, respectively. Moreover, the yield curve appears to level off between ~ 40 and ~ 50 eV (level *C*); then a steady decline is resumed above ~ 50 eV.

The present yield curve is quite different from that of Hertel et al. [1]. Their spectrum displays essentially no marked structures at 35 eV ≥ $h\nu$ ≥ 23 eV. Our ion yield curve is similar to the photoabsorption cross section of C_{60} calculated by Colavita et al. [2], i.e. the dotted line in Fig. 1 They demonstrated that the shape resonances give rise to fine structures in the cross section curve. Comparing the solid and dotted curves gives us the following summarization: (1) peak *A* observed at 26 eV can be identified to the peak at 27 eV in the calculated spectrum, (2) peak *B* observed at 34 eV probably has the same origin as the calculated shoulder around 32 eV, and (3) level *C* between ~ 40 and ~ 50 eV is compatible with the calculated flat region from 35 to 45 eV. The good agreement between the solid and dotted curves in Fig. 1.strongly supports that the observed fine structures are due to ionization via the shape resonances as single electron excitation to vacant orbitals. Conversely there is no tangible evidence in favor of the plasmon resonance, that is collective electron excitation.

Above 50 eV the relative ion yield curve is reasonably represented by the absorption cross section of a carbon atom as evidenced by the dashed curve in Fig. 1. In this region the photoionization cross sections are dominated by ionization from deeper orbitals described by linear combinations of compact carbon 2*s*-type orbitals, so that the relative ion yield of C_{60}^{+} from C_{60} agrees well with the absorption cross section of a carbon atom.

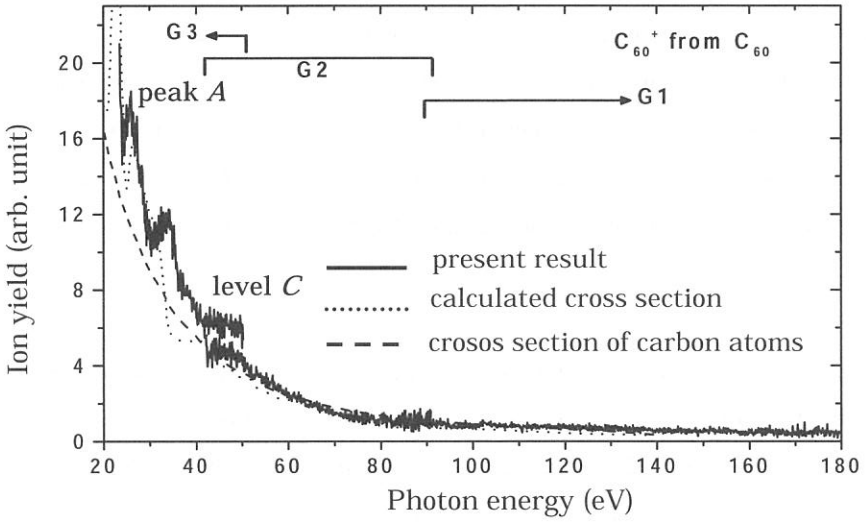

References

[1] I. V. Hertel, H. Steger, J. de Vries, B. Weisser, C. Menzel, B. Kamke and W. Kamke, Phys. Rev. Lett. **68** (1992) 784.

[2] P. Colavita, G. De Alti, G. Fronzoni, M. Stener and P. Decleva, Phys. Chem. Chem. Phys. **3** (2001) 4481.

[3] J. Kou, T. Mori, M. Ono, Y. Haruyama, Y. Kubozono and K. Mitsuke, Chem. Phys. Lett. in press.

[4] T. Mori, J. Kou, M. Ono, Y. Haruyama, Y. Kubozono and K. Mitsuke, submitted to Rev. Sci. Inst.

[5] M. Ono, H. Yoshida, H. Hattrori and K. Mitsuke, Nucl. Instrum. Meth. Phys. Res. A **467-468** (2001) 577.

(BL2B2)

Development of a Photoionization Spectrometer for Precise Ion Yield Measurements from Gaseous Fullerenes

T. Mori,[a] J. Kou,[a] M. Ono[a], Y. Haruyama,[b] Y. Kubozono[a,b], and K. Mistuke[a),c),]

[a] *Department of Vacuum UV photo-science, Institute for Molecular Science, Myodaiji, Okazaki 444-8585, Japan*

[b] *Department of Chemistry, Faculty of Science, Okayama University, Okayama 700-8530, Japan*

[c] *Graduate University for Advanced Studies, Myodaiji, Okazaki 444-8585, Japan*

Geometrical structures and electronic properties of fullerenes have attracted widespread attention because of their novel structures, novel reactivity, and novel catalytic behaviors as typical nano-size materials. Moreover, it has been emphasized that the potential for the development of fullerenes to superconductors and strong ferromagnetic substances is extremely high. In spite of such important species spectroscopic information is very limited in the extreme UV region.

In the present study, we tried to develop a new apparatus for obtaining reliable photoion yield curves for fullerenes with improved statistics in the range of extreme UV region. For this purpose, several essential devices have been introduced and exploited in combination with a high-temperature source of gaseous fullerenes: a grazing-incidence monochromator, a conical nozzle, a quartz-oscillator thickness monitor, and an efficient time-of-flight mass spectrometer. We have examined their performance by using C_{60} [1].

The sample of C_{60} with 99.98% purity was purchased and further purified by eliminating the organic solvent such as benzene or toluene through heating the sample one day in vacuum at 300 °C. Every experiment has been performed by using an 18 m spherical grating monochromator with high resolution and high photon flux installed at beamline BL2B2 of the UVSOR facility. The performance of the monochromator was described in ref. [2].

Figure 1 illustrates the side view of the high-temperature oven supplying gaseous fullerenes and that of the photoionization mass spectrometer. A copper sample holder attached to a conical nozzle was mounted inside a radiation shield made of stainless steel. The fullerene sample was loaded into the sample holder which was resistively heated. The oven temperature was measured by a chromel-alumel thermocouple fitted to the bottom of the sample holder. We employed a water-cooled thickness monitor placed 35 mm away from the central point of the ionization region for the purpose of measuring the flux of the fullerene beam correctly. Gaseous fullerenes were subjected to irradiation of the synchrotron radiation from the Dragon-type monochromator. Photoions traversed a drift tube of 71 mm in length and were detected with a microchannel plate electron multiplier detector (MCP). We could accordingly obtain a TOF mass spectrum of the fullerene ions. Insertion of the drift tube allows us to drastically reduce the background counts due to stray electrons and impurities and then realize a stable operation of the MCP detector. The drift tube was equipped with parallel plate electrodes, designated in Fig. 1 as a repeller and an extractor, placed above the oven unit. A pulse voltage rising from the ground level to +100 V was applied to the ion repeller electrode as a start trigger for the TOF measurements. In the case of C_{60}, the duration and frequency of this pulse voltage were 3 μs and 5 kHz, respectively.

A TOF mass spectrum demonstrates three broad peaks, which are assignable to singly, doubly and triply charged cations of C_{60}. Figure 2 shows the photoionization efficiency curve of C_{60}^+ produced from C_{60}. The spectrum displays a tendency to decrease gradually with increasing photon energy, since this region is located on the higher energy side of the prominent resonance at $h\nu \sim 20$ eV.[3] Two distinct peaks are found at $h\nu = 26$ and 34 eV, and there is a flat area between ~ 40 and ~ 50 eV. Hertel et al.[3] have reported the ionization efficiency of C_{60}^+ from C_{60} ranging from 7.5 to 35 eV, but their result appreciably differs from our efficiency curve probably due to difference in statistics at $h\nu > 25$ eV. Colavita et al.[4] have calculated a theoretical photoabsorption cross section curve of C_{60}, which exhibits several peaks and shoulders above 25 eV. Their cross section curve shows a good agreement with our result.

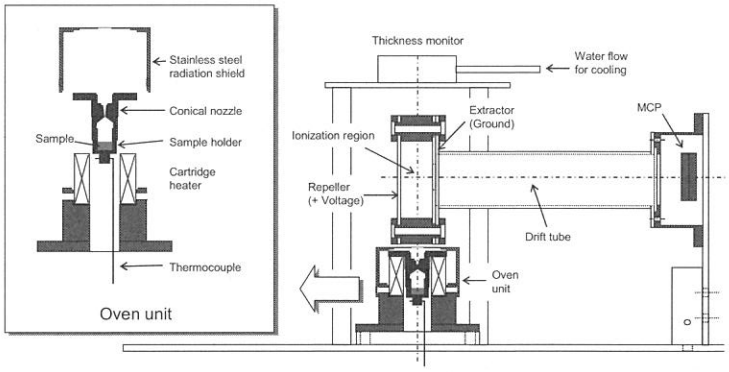

Fig. 1 Apparatus of the photoionization spectrometer and an expansion of the oven unit.

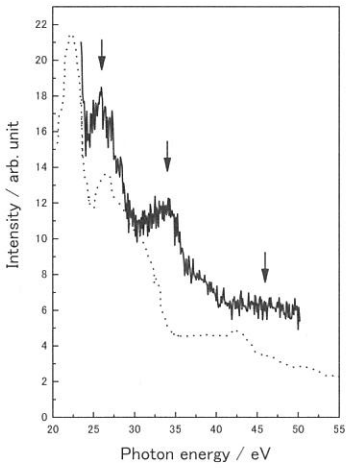

Fig. 2 Photoionization efficiency curve of C_{60}^+ produced from C_{60}. Tow peaks and a flat area are indicated by the arrows. The doted line designates the theoretical photoabsoption cross section reported by Colavita et al. (Ref. 3).

References

[1] T. Mori, J. Kou, M. Ono, Y. Haruyama, Y. Kubozono and K. Mitsuke, submitted to *Rev. Sci. Instrum.*.

[2] M. Ono, H. Yoshida, H. Hattori and K. Mitsuke, *Nucl. Instrum. Methods* A. **467**, 577 (2001).

[3] I. V. Hertel, H. Steger, J. D. Vries, B. Weisser, C. Menzel, B. Kamke and W. Kamke, *Phys. Rev. Lett.* **68,** 784 (1992).

[4] P. Colavita, G. D. Alti, G. Fronzoni, M. Stener and P. Decleva, *Phys. Chem. Chem. Phys.* **3**, 4481 (2001).

(BL2B2)

Anisotropy of Fragment Ions from SF_6 by Photoexcitation between 23 and 210 eV

Masaki Ono [a] and Koichiro Mitsuke [b]

[a] *Center for Advanced Microstructures and Devices, Louisiana State University, 6980 Jefferson Highway, Baton Rouge, LA 70806, U.S.A.*

[b] *Institute for Molecular Science, Myodaiji, Okazaki 444-8585, Japan*

Department of Structural Molecular Science, The Graduate University for Advanced Studies

The anisotropy of the fragment ions produced by photoexcitation of SF_6 has been measured using synchrotron radiation in the energy range of 23 – 210 eV [1]. The apparatus for measuring the angular distribution of the fragment ions has been newly constructed. Two sets of detection system are composed of an ion detector and preceding three grids, as shown schematically in Fig. 1.

In spite of the highly symmetrical molecule strong anisotropy is observed at lower photon energies. Figure 2 shows the fragment ion yield from SF_6 and the relevant β in the energy region of E_{hv} = 23 - 210 eV. Anisotropy gradually decreases with increasing photon energy.

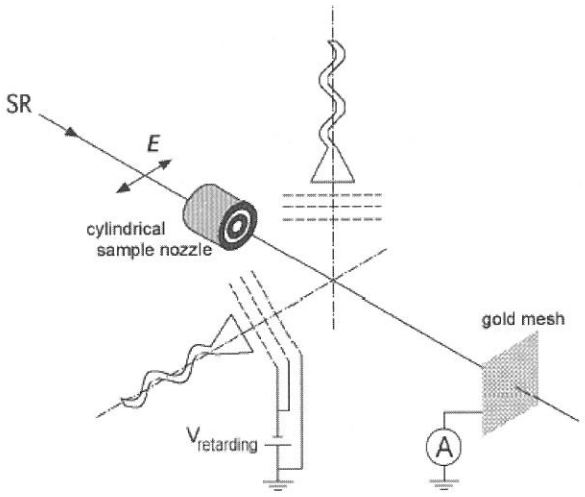

Figure 1. Schematic experimental setup for the measurement of anisotropy of fragment ions. Two sets of ion detection system are mounted in the parallel and perpendicular directions with respect to the electric vector of synchrotron radiation.

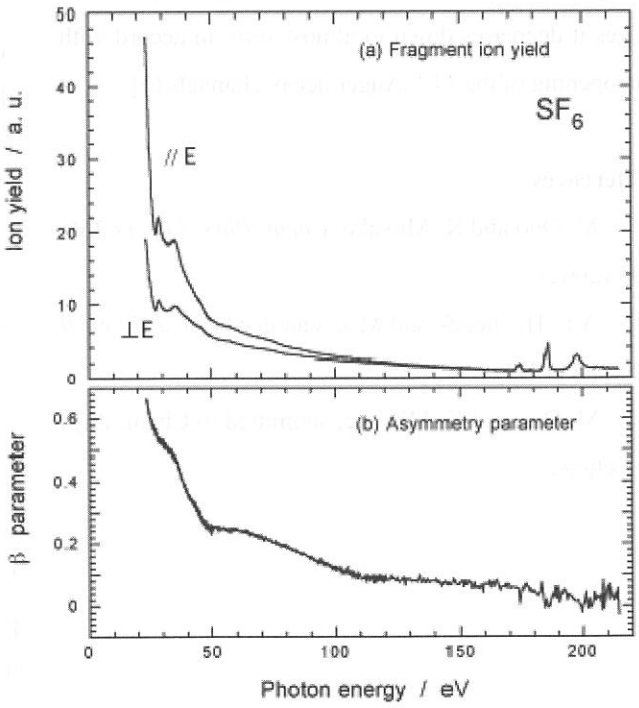

Figure 2. (a) Yield spectrum and (b) asymmetry parameter for all the fragment ions from SF_6 measured at E_{hv} = 23 – 210 eV.

The behavior of the curve of the asymmetry parameter has been interpreted qualitatively by means of simulation using partial oscillator strengths for the formation of fragment ions in the region of valence electron excitation (16 - 63 eV) as illustrated in Fig. 3. Only SF_5^+ ions are assumed to have an anisotropic angular distribution, which can be explained in terms of transitions into neutral excited states of valence type. With increasing photon energy the branching ratio for the SF_5^+ ion decreases [2], while the contribution of direct photoionization may increase. As a result the asymmetry parameter involving all the fragment ions declines steadily with the photon energy. Moreover, inner valence-electron excitation between 35 and 50 eV is found to open new decay channels which produce photoions isotropically.

Fragment ion yield spectrum and β parameter around the ionization edge of the sulfur $2p$ electron are shown in Fig. 4. The asymmetry parameter remains constant at 0.01 – 0.02 below the sulfur $2p_{3/2,1/2}$ edges (<180 eV), whether the photon energy is chosen at on- or off-resonance. Above the edges it decreases down to almost zero, in accord with the opening of the *LVV* Auger decay channels [3].

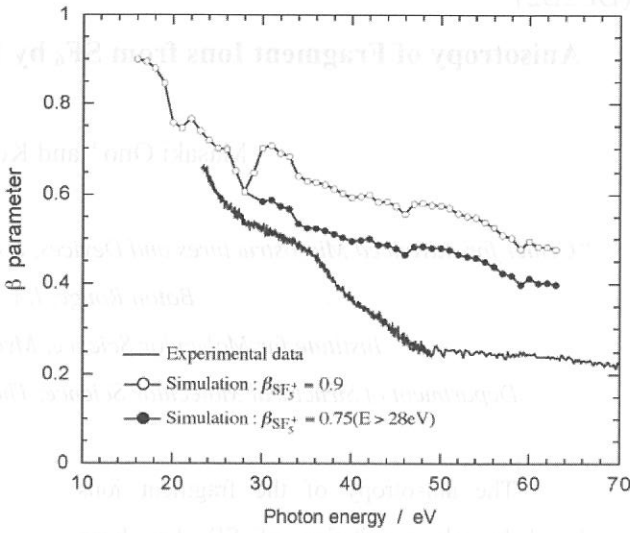

Figure 3. Asymmetry parameter for all the fragment ions from SF_6 at E_{hv} = 16 – 70 eV. Solid line and symbols show the experimental and simulation data, respectively. ○: Calculated at E_{hv} = 16 - 63 eV by assuming that the asymmetry parameter for SF_5^+ is constant, i.e. $\beta_{SF_5^+} = 0.9$. ●: Calculated at E_{hv} > 28 eV by assuming that $\beta_{SF_5^+}$ drops to 0.75 above 28 eV. The lines connecting the simulation data points are to guide the reader's eye.

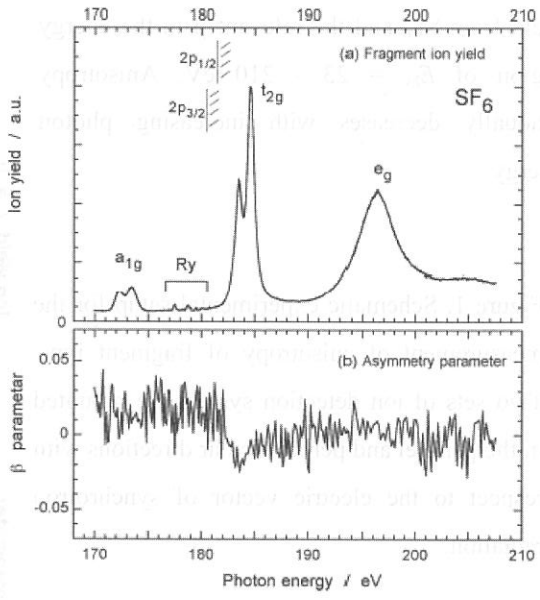

Figure 4. (a) Yield spectrum and (b) asymmetry parameter for all the fragment ions from SF_6 around the ionization edges of the sulfur $2p$ electron.

References

[1] M. Ono and K. Mitsuke, *Chem. Phys. Letters* **366,** 595 (2002).

[2] A.P. Hitchcock and M.J. Van der Wiel, *J. Phys. B* **12** 2153 (1979).

[3] M. Ono and K. Mitsuke, submitted to Chem. Phys. Letters.

(BL3A2)

Dissociative Photoionization of NO_2 in the Range from 37 to 125 eV

T. Masuoka

Department of Applied Physics, Graduate School of Engineering, Osaka City University, Sugimoto 3-3-138, Sumiyoshi-ku, Osaka 558-8585

Molecular and dissociative photoionization of NO_2 has been studied in the photon-energy region of 37-125 eV by use of time-of-flight (TOF) mass spectrometry and synchrotron radiation. Ion branching ratios were obtained by analyzing TOF mass spectra for the singly charged NO_2^+, NO^+, O^+, and N^+ ions as well as doubly charged N^{2+} and O^{2+} ions and were converted to the absolute partial cross sections by using the reported total absorption cross section of NO_2 [1]. Experimental details can be found elsewhere [2].

The present results are shown in Figs. 1 and 2 in comparison with those reported by Au and Brion [1]. It can be seen in Fig. 1 that the NO^+ ion is the major product in the energy region studied (the branching ratio is 0.567 at 37 eV) and gradually decreases as the excitation energy increases. The parent NO_2^+ ion is the minor product (the branching ratio is 0.148 at 37 eV) and also slightly decreases at higher photon energies. On the other hand, the ion branching ratios for O^+ and N^+ continue to increase in the energy regions of 37-120 eV and 50-120 eV, respectively. The production of the doubly charged fragment ions, N^{2+} and O^{2+}, is discernible above 60 eV (the threshold for both ions), although these ion branching ratios are less than about 0.1%. As for the thresholds of N^{2+} and O^{2+}, electron-impact experiments have reported to be about 80 eV (N^{2+} and O^{2+} are not resolved) [3], and 51.5 ± 1 eV for N^{2+} and 52.1 ± 1 eV for O^{2+} [4], which should be compared with the present value.

The observation of the O_2^+ ion has been reported by Au and Brion (the abundance is ~1%) and by other experiments [5,6], whereas the majority of reported experiments including photoionization mass spectrometry [7] and electron impact studies [7] has not reported the presence of O_2^+ in the respective mass spectra in accordance with the present results. This issue may remain as an open question. The discrepancies in the ion branching ratios for NO_2^+, O^+, and N^+ between the present results and those of Au and Brion can be seen in Fig. 1, although their energy dependencies are quite similar in both results. These discrepancies are mainly due to the application of mass sensitivity correction factors determined for the ion detector to the ion fragmentation branching ratios obtained from the TOF mass spectra of Au and Brion. Cooper *et al.* [8] determined mass sensitivity correction factors for a microchannel-plate detector (as well as a Johnston multiplier) by using rare gas atoms He, Ne, Ar, Kr, and Xe and found that significant variations in detector sensitivity occur at low *m/e* values. Their results have been applied to the ion branching ratios of Au and Brion for NO_2. Therefore, the correction factors for the N^+ and O^+ production from NO_2 are large, causing the discrepancies for both ions between the two data sets shown in Fig. 1. The discrepancy for O^+ between the two data sets is in the range of 1.04-1.13 (the ion branching ratio of Au and Brion over the present ion branching ratio), and for N^+ it is about 1.15 throughout the energy region that the present data cover, which are very close to the sensitivity correction factors adopted by Au and Brion. However, as pointed out by Cooper *et al.* [8], the detection efficiencies for atomic, diatomic, and polyatomic ions of the same *m/e* may be different and the application of the correction factors obtained for rare gas ions to the case of NO_2 is questionable. The differences in the ion branching ratios for N^+ and O^+ between the two data sets causes rather large differences in the branching ratios of NO_2^+, ranging 0.73-0.65 (Au and Brion/present). The reason that only the ion branching ratio for NO_2^+ is affected and the ion branching ratios for NO^+ of the two data sets are in good agreement is not clear at present.

The present partial photoionization cross sections were obtained by the use of Eq. 5 [2], that

is, the product of the ion branching ratio, the ionization yield, and the total absorption cross section. The results for the major ions are shown in Fig. 2 in comparison with those of Au and Brion. It should be noted that Au and Brion used the ionization yield of unity above 24.5 eV (even in the energy region that dissociative double ionization takes place), whereas in the present data the ionization yield ranges 1.00-1.185 in the region from the double photoionization threshold (35.0 eV) to 125 eV, as will be reported elsewhere. Because of the large discrepancy in the ion branching ratios of NO_2^+ mentioned above, the partial cross section for NO_2^+ is obviously different between the two data sets.

References

[1] J. W. Au and C. E. Brion, Chem. Phys. **218**, 109 (1997).
[2] T. Masuoka *et al.*, J. Chem. Phys. **109**, 2246 (1998).
[3] B. G. Lindsay *et al.*, J. Chem. Phys. **112**, 9404 (2000).
[4] A. S. Newton and A. F. Sciamanna, J. Chem. Phys. **52**, 327 (1970).
[5] R. V. Hodges *et al.*, Int. J. Mass Spectrom. Ion Phys. **39**, 133 (1981).
[6] J. H. D. Eland and L. Karlsson, Chem. Phys. **237**, 139 (1998).
[7] see references in [1].
[8] G. Cooper *et al.*, Rev. Sci. Instrum. **64**, 1140 (1993).

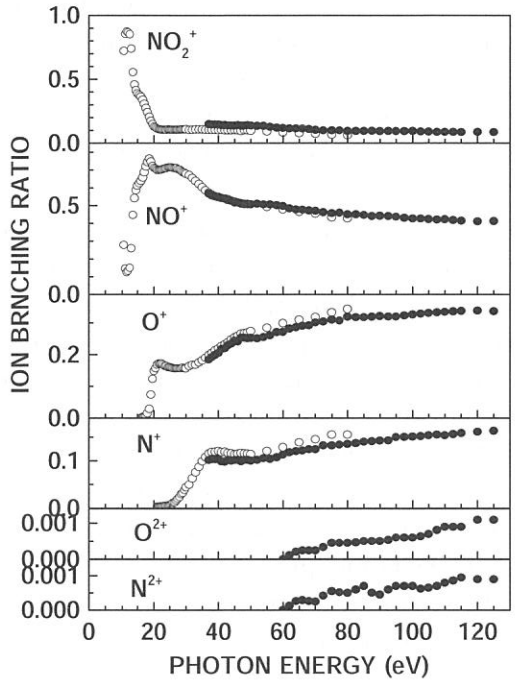

Fig. 1 Ion branching ratios of NO_2
•; present results, ○; from [1].

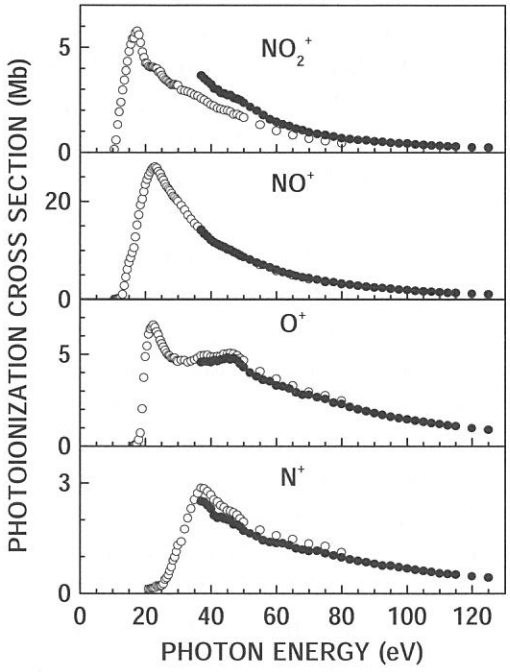

Fig. 2 Partial cross sections of NO_2
•; present results, ○; from [1].

(BL3A2)

Dissociation Mechanism of H_2O into $OH^+(\tilde{A}\,^3\Pi_\Omega)$ + H(n=1) Manifested by Ultraviolet Dispersed Spectroscopy

Koichiro Mitsuke

Institute for Molecular Science, Myodaiji, Okazaki 444-8585, Japan

Department of Structural Molecular Science, The Graduate University for Advanced Studies

The photofragmentation of H_2O has been studied by fluorescence spectroscopy at photon energies between hν = 16.9 – 54.5 eV. The primary photon beam was monochromatized undulator radiation supplied from BL3A2 of the UVSOR facility. The fluorescence in the wavelength range of 280 – 720 nm was dispersed with an imaging spectrograph. The appearance energy of the $OH^+(\tilde{A}\,^3\Pi_\Omega, v' \rightarrow \tilde{X}\,^3\Sigma^-, v'')$ transitions is found to be ca. 25.5 ± 0.3 eV. This value is much higher than the dissociation limit for the $OH^+(\tilde{A}\,^3\Pi_\Omega)$ + H(n=1) channel, but is consistent with the vertical ionization energy to $H_2O^+[(1b_1)^{-2}(4a_1)^1\,^2A_1]$ that has been assumed to correlate with the above dissociation limit in the literature. The vibrational distribution of $OH^+(\tilde{A}\,^3\Pi_\Omega)$ is similar to the prior distribution in the rigid-rotor harmonic-oscillator approximation.

Figure 1 shows an emission spectrum encompassing the λ = 280 – 420 nm range, in which many vibrational bands of the $OH^+(\tilde{A}\,^3\Pi_\Omega, v' \rightarrow \tilde{X}\,^3\Sigma^-, v'')$ transitions can be identified. The right and left figures in parentheses designate, respectively, the upper v' and lower v'' vibrational levels of OH^+. The v' level ranges from zero to three.

The lowest thermochemical threshold of H_2O for the formation of $OH^+(\tilde{A}\,^3\Pi_\Omega)$ is evaluated to be 21.5 eV, corresponding to dissociation into $OH^+(\tilde{A}\,^3\Pi_\Omega)$ + H(n=1). Our results, however, indicate that the $OH^+(\tilde{A}\,^3\Pi_\Omega)$ fragments are scarcely produced at hν = 21.7 and 24.9 eV. To make this point clearer the fluorescence intensity was measured as a function of hν in the wavelength region λ = 356 - 364 nm. This region includes the (0,0) vibrational band of the $OH^+(\tilde{A}\,^3\Pi_\Omega \rightarrow \tilde{X}\,^3\Sigma^-)$ transition. The resultant fluorescence excitation spectrum of H_2O is depicted in Fig. 2. The intensity shows a slow onset at 25.5 ± 0.3 eV. which is much higher than the dissociation limit of 21.5 eV and can be interpreted in terms of a highly repulsive PES of the excited H_2O^+ state along the dissociation coordinate. The correlation diagram of H_2O^+ proposed by Appell and Durup manifests that

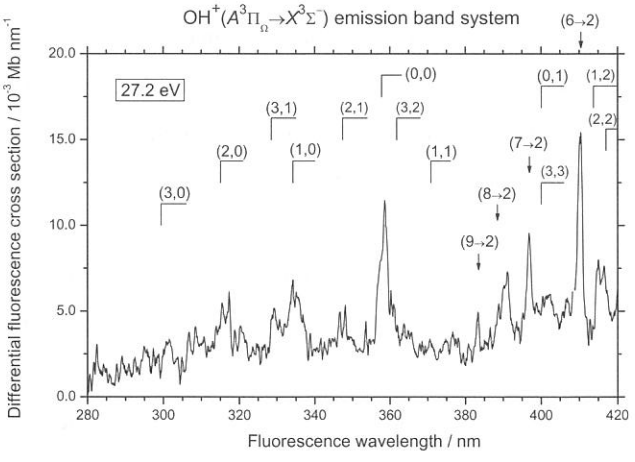

Figure 1. Dispersed fluorescence spectrum of H_2O at E_{hv} = 27.2 eV. The vertical lines indicate the band origins of the $OH^+(\tilde{A}\,^3\Pi_\Omega, v' \rightarrow \tilde{X}\,^3\Sigma^-, v'')$. The ($v'$, v'') marks denote the bands due to the transition from the upper v' to lower v'' vibrational states.

the $OH^+(\tilde{A}\,^3\Pi_\Omega)$ + H(n=1) limit correlates with a 2-hole 1-particle $^2A_1$ state of H_2O^+ with the electronic configuration of $[(1b_1)^{-2}(4a_1)^1]$. This doubly excited $H_2O^+(^2A_1)$ state was reported to be located at 27.6 ± 1 eV with respect to $H_2O(\tilde{X}\,^1A_1)$ in the Franck-Condon region. This vertical ionization energy rationalizes the present observation that the $OH^+(\tilde{A}\,^3\Pi_\Omega \rightarrow \tilde{X}\,^3\Sigma^-)$ band system begins to appear at hν = 25.5 eV.

We have calculated the vibrational distribution of the fluorescing $OH^+(\tilde{A}\,^3\Pi_\Omega)$ fragments for the purpose of obtaining a clue to energy partitioning when the system runs down the PES of $H_2O^+[(1b_1)^{-2}(4a_1)^1\ ^2A_1]$. The cross section for each vibrational band can be connected with the vibrational distribution $P_{v'}$ by

$$\sigma_{v'v''} \propto P_{v'}\, q_{v'v''}\, \nu^3_{v'v''}\, R_e(\bar{r}_{v'v''})^2. \qquad (1)$$

Here, $q_{v'v''}$ denotes the Franck-Condon factor with regard to the $OH^+(\tilde{A}\,^3\Pi_\Omega \rightarrow \tilde{X}\,^3\Sigma^-)$ transition, $\nu_{v'v''}$ the transition frequency, and R_e the electronic transition moment at the r-centroid $\bar{r}_{v'v''}$ of the relevant vibrational transition (v',v''). We adopt the following linearly decreasing function of R_e^2 with increasing $\bar{r}_{v'v''}$ proposed by Gérard *et al.*:

$$R_e(\bar{r}_{v'v''})^2 = 4.02 - 27.65\,\bar{r}_{v'v''}, \qquad (2)$$

where $\bar{r}_{v'v''}$ is in nm. The (0,0), (1,0), (2,1), and (3,1) vibrational bands are chosen for calculating $P_{v'}$ from the peak area by using Eq. (1). The calculated distribution is illustrated in Fig. 3. As the statistical limit the prior distribution $P^0_{v'}$ in the rigid-rotor harmonic-oscillator approximation is evaluated from the relation

$$P^0_{v'} \propto (1 - f_{v'})^{1.5}, \qquad (3)$$

and plotted in Fig. 3 as well. Here, $f_{v'}$ is the vibrational fraction of the available energy of 5.7 eV (= 27.2 - 21.5). The two distributions are in a good agreement with each other, suggesting that statistical factors dominate the partitioning of the available energy into the vibronic degrees of freedom of the $H_2O^+[(1b_1)^{-2}(4a_1)^1\ ^2A_1]$ state.

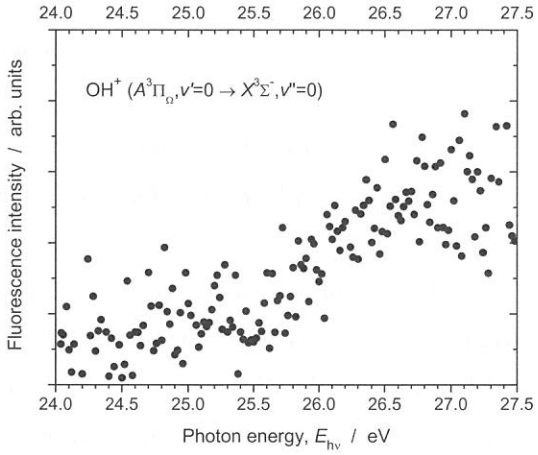

Figure 2. Fluorescence excitation spectrum of H_2O obtained by plotting the fluorescence intensity integrated over the wavelength region of 356 – 364 nm as a function of hν.

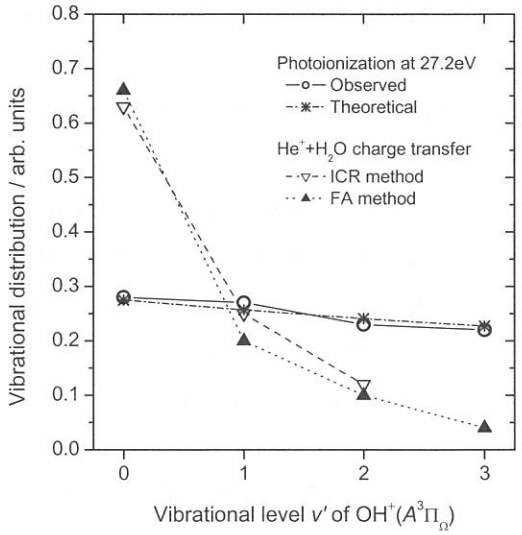

Figure 3. Observed (○) and theoretical (✳) vibrational distributions of the $OH^+(\tilde{A}\,^3\Pi_\Omega, v')$ state produced by photoionization of H_2O at hν = 27.2 eV. The former distribution is calculated from the peak area of the vibrational bands in Fig. 1. The latter is the prior distribution given by Eq. (3). The distributions in the $He^+ + H_2O$ charge transfer reaction measured by ICR and flowing afterglow methods are indicated by the ▽ and ▲ symbols, respectively.

Reference

[1] K. Mitsuke, *J. Chem. Phys.* **117,** 8334 (2002).

(BL3A2)

Development of the Laser – SR Combination technique on Photodissociation Studies of Highly Excited Vibrational Molecules

Koichiro Mitsuke

Institute for Molecular Science, Myodaiji, Okazaki 444-8585, Japan

Department of Structural Molecular Science, The Graduate University for Advanced Studies

It is possible that vibrationally mediated photodissociation is performed by using laser and synchrotron radiation. Namely, infrared or visible laser is primarily used to excite a selected vibrational level in the electronic ground state, and then synchrotron radiation is irradiated to promote photoexcitation. Figure 1 illustrates the absorption spectrum of a vibrationally excited molecule in a one-dimensional model system. Here, $V_0(R)$ and $V_1(R)$ denote the potentials in the ground and excited electronic states, and $\Psi_i(R)$ the initial wavefuction. From the reflection principle the absorption cross section can be represented by these equations:

$$V_1(R_t) = E, \qquad \sigma(E) \approx \frac{|\Psi_i(R_t)|^2}{\left|dV_1/dR\right|_{R=R_t(E)}}$$

Here, R_t stands for the classical turning point. The cross section is a reflection of the initial distribution of $|\Psi_i(R)|^2$ onto the energy axis mediated directly by the upper-state potential. Therefore, multi-modal reflection structures appear in the spectrum when two or more vibrational quanta are initially excited.

In the two-dimensional case, an analogous multi-modal structure can be seen when the parent molecule is excited in the direction of the dissociation path. On the contrary, nodes along the line perpendicular to the dissociation path do not lead to reflection structures. Water and its isotope-substituted HOD are the two most prototypical molecules whose photodissociation of highly excited vibrational states has been well studied.

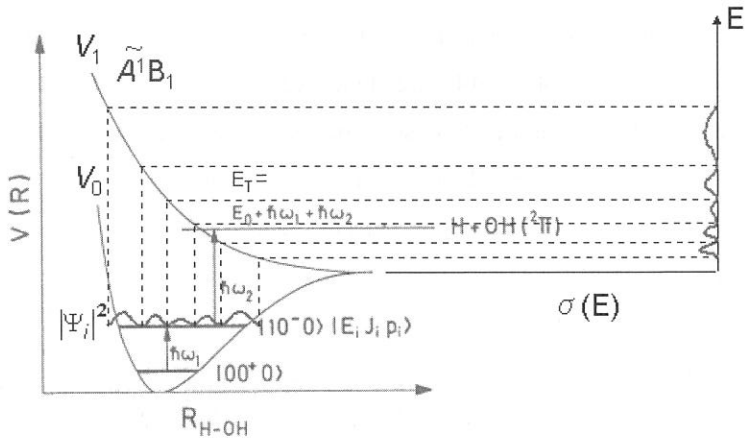

Figure 1. Absorption spectrum of a vibrationally excited molecule in a one-dimensional model system.

It has been documented that the initial vibrational excitation influences the chemical branching, if two different dissociation channels can be accessed. Much attention has been focused on the pioneering work of Crim and his collaborators [1], who could accomplish the selective bond-breaking of heavy water, HOD. Very recently, Akagi and coworkers reports that deuterized ammonia NHD_2 in the fourth N-H stretching overtone preferentially photodissociates into the ND_2 + H channel [2].

In these studies UV lasers have been employed for vibrationally mediated photodissociation. Instead, I am planning to use synchrotron radiation in the vacuum UV region because of the following interests:

(1) Elucidating the properties of dissociative states in the vacuum UV region by sampling a wide range of their potential energy surfaces, such as dynamics determining the final-state distributions of the products, nonadiabatic transitions on dissociation, and assignments and characterization of unknown multiply-excited states produced by Auger decay from core-excited states.

(2) Aiming at more universal "vibrational state-specific" rupture of chemical bonds, by changing the overlap of the upper-state continuum wavefucntions with the ground-state wavefunction.

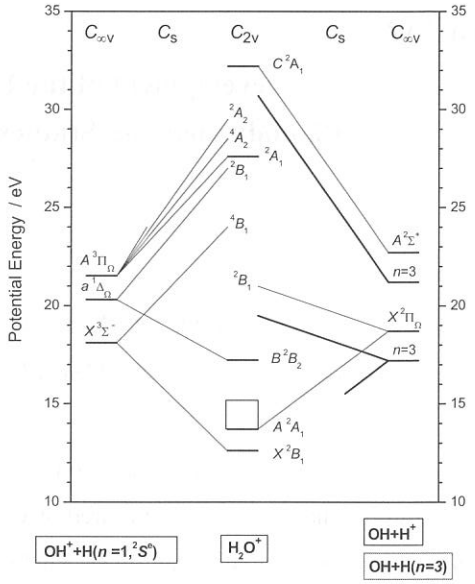

Figure 2. Correlation diagram between H_2O^+ and OH^+ + H and between H_2O^+ and OH + H^+.

We tried to select an appropriate excited state through which photodissociation of vibrationally excited molecules can be investigated based on the correlation diagram in Fig. 2 that we proposed in [3]. First, we tackled the two $^2A_1$ states which correlate the $OH^+(A^3\Pi_\Omega)$ + H(n=1) and OH $(A^2\Sigma^+)$ + H^+ limits. Since these states are highly repulsive, it is likely that significant decrease in the appearance energy for the formation of the photofragments is perceived, by setting vibrationally excited molecules to the initial state of photodissociation. We probed the final fragments by observing spontaneous emission from $OH^+(A^3\Pi_\Omega)$ or OH $(A^2\Sigma^+)$.

A continuous titanium-sapphire laser was used in the wavenumber range between 13814 – 13819 cm^{-1}, with its bandwidth of 4×10^{-4} cm^{-1} and scanning range of 30 GHz. This energy range corresponds to excitation of the third O-H stretching overtone of water. However, when the visible laser was introduced, no additional peak feature of emission bands has been detected in the dispersed spectra. Then I changed my mind to shift the target to the dissociation channel of $OH^+(X^3\Sigma^-)$ + H(n=1). The OH^+ ion was detected with quadrupole mass spectrometer. Figure 3 shows the difference between the normalized signal ion counts with and without the visible laser. Measurements were fulfilled at SR photon energies near the dissociation threshold of 18.05 eV. We consider that the curve exhibits multi-modal reflection structures due to the nodes of the vibrational wave function of the $4\nu_{O\text{-}H}$ stretch overtone of H_2O.

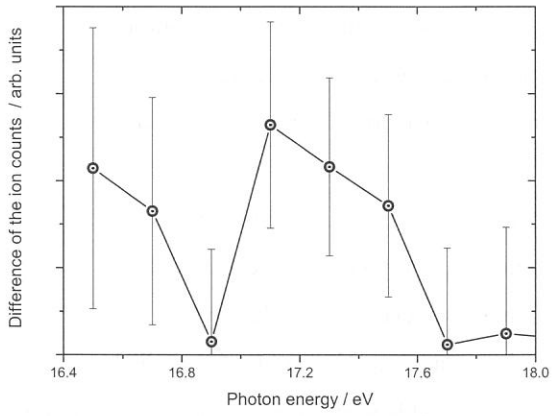

Figure 3. Difference between photoionization efficiencies for OH^+ + H from H_2O with and without the laser.

References

[1] R.L. Vander Wal, J.L. Scott and F.F. Crim, *J. Chem. Phys.* **92,** 803 (1990).

[2] H. Akagi, K. Yokoyama and A. Yokoyama, *J. Chem. Phys.* **118,** 3600 (2003).

[3] K. Mitsuke, *J. Chem. Phys.* **117,** 8334 (2002).

(BL4B)

Ar 2p Excited States of Argon in Non-Polar Matrix

Takaki Hatsui, Mitsuru Nagasono*, Nobuhiro Kosugi

Institute for Molecular Science, Myodaiji, Okazaki 444-8585
** Dept. of Materials Science and Engineering, Kyoto University, 606-8501, Japan*

Rydberg states in condensed phase are of interest because they are sensitive to external perturbation due to their large orbital radii. Rare gas (Rg) matrices have mostly been used to investigate the Rydberg states of atomic and molecular Rydberg states. A systematic study of NO molecule in rare gas, N_2 and H_2 matrices on the first ionization threshold has been reported [1]. In the core excitation region, rare gas media in cluster have extensively studied [2,3]. In the present study, core-excited Rydberg states of Ar in Rg and N_2 matrices (Ar/Rg, Ar/N2) have been investigated by photoabsorption spectroscopy.

Photoabsorption spectra were measured by a partial electron yield (Auger yield) method using a MCP detector with a retarding mesh. Photon energy was calibrated by measuring Ar $2p_{3/2}$-4s* peak (244.4 eV) of Ar in gas phase in transmission mode before and after each measurement. Samples were prepared by introducing mixed gas of Ar and Rg (or N_2) onto Au coated copper plate of a cryostat. The mixed gas is dosed approx. 30 L. The temperature of the copper plate was below 9 K. All spectra were taken at grazing incidence angle of 15 degree.

Fig. 1 shows Ar L-edge photoabsorption spectra for Ar/Rg and Ar/N_2 with atomic (molecular) ratio of Ar:Rg (N_2)=1:4. Compared with the Ar gas spectrum, the lowest band, Ar solid spectrum show broadened Ar $2p_{3/2}$-4s band with a shoulder structure at the lower energy side. In order to discriminate surface contribution from bulk, fluorescence yield (F.Y. dotted line) was measured for solid Ar. In fluorescence yield spectra, the shoulder was clearly suppressed in intensity and hence assigned to the Ar $2p_{3/2}$->4s excitation of surface Ar atoms, which is in accord with the previous assignment for Ar cluster[4]. The excitation energy for bulk $2p_{3/2}$->4s band is blue shifted in a sequence of Ar/Xe, Ar/Kr, and solid Ar. Neighboring atoms with shorter interatomic distance are expected to have larger perturbation because the excited electron in Rydberg states is push to higher energy side by closer potential of the surrounding atoms. Similar trend is observed for samples with different Ar concentration (Fig. 2-3), i.e. lower Ar concentration in Ar/Rg system results in lower excitation energy because of longer Ar-Rg length in Ar/Kr and Ar/Xe systems.

In the case of Ar/Xe, Ar $2p_{1/2}$-4s and Ar $2p_{3/2}$ nd states are merged into a broad band, which imply that nd series form band structure by significant overlap with the neighboring atoms. The broad band split in Ar/Kr and Ar solid and form two distinct bands in Ar/N_2, which indicates that nd series interact with neighbors more strongly than 4s Rydberg states. This can be explained as stronger repulsion by the surrounding atoms arises from larger radii of nd Rydberg series than 4s Rydberg states.

References

1. M. Chergui et al., J. Chem. Phys., 91 (1989) 5993.
2. E. Rühl et al., J. Chim. Phys. Phys.-Chim. Biol., 92 (1995) 521.
3. O. Björneholm, Surface Review and Letters, 9 (2002) 3.
4. E. Rühl et al., J. Chem. Phys., 98 (1993) 6820.

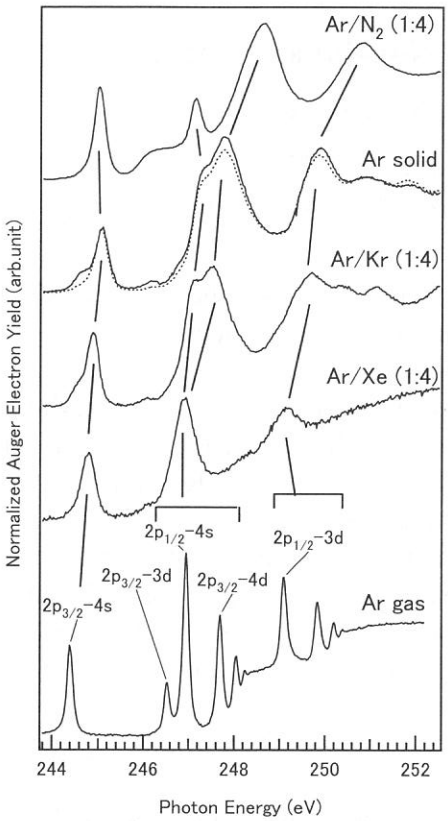

Fig. 1. Ar L-edge photoabsorption spectra for Ar gas, Ar solid (Auger yield and florescence yield), Ar/Xe, Ar/Kr and Ar/N_2.

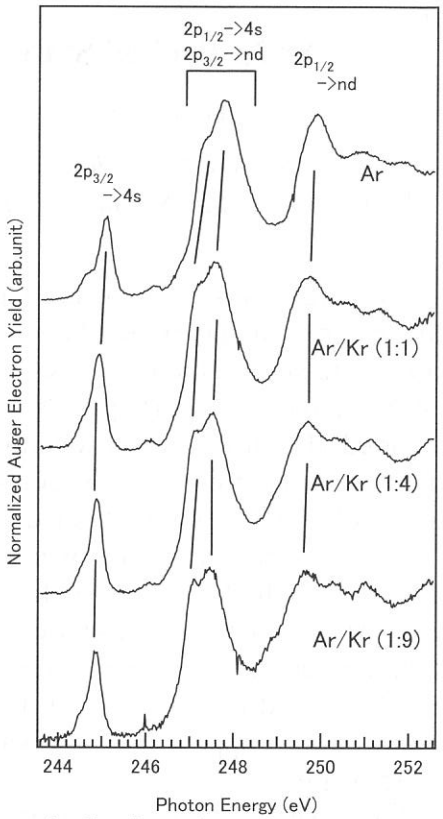

Fig. 2. Ar L-edge photoabsorption spectra of Ar in Kr matrix.

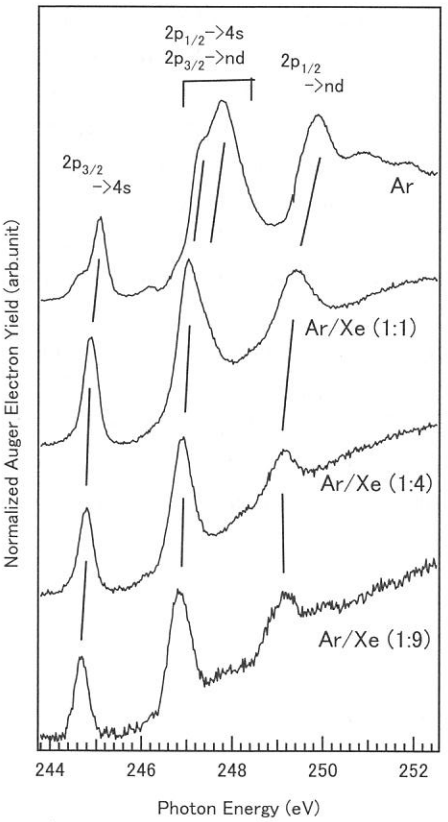

Fig. 3. Ar L-edge photoabsorption spectra of Ar in Xe matrix.

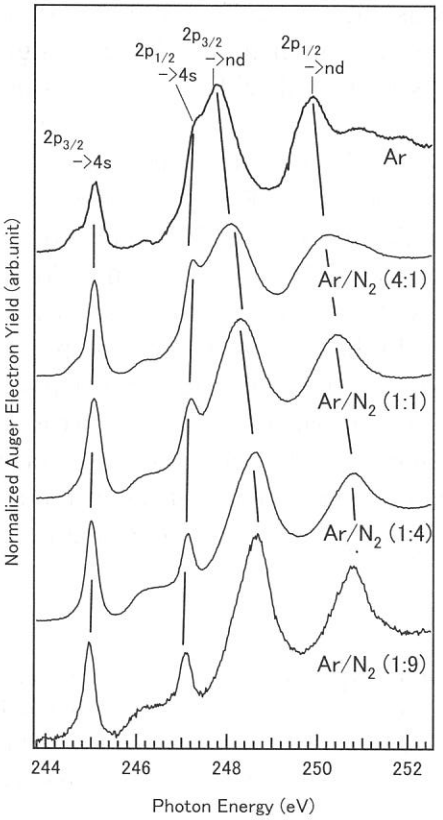

Fig. 4. Ar L-edge photoabsorption spectra of Ar in N_2 matrix.

(BL4B)

Development of a new spectroscopic technique for probing multielectron processes in molecules

Tatsuo GEJO, Eiji SHIGEMASA, Eiken NAKAMURA

Institute for Molecular Science, Myodaiji, Okazaki 444-8585, Japan

Introduction

The dynamics of molecular inner-shell photoexcitation, photoionization, and subsequent decay processes is much more complex, in comparison to outer-shell photoionization which is still largely within the scope of the single electron picture. For instance, the excitation and ionization of valence electrons accompanies the inner-shell photoionization, which manifest themselves as shake-up and shake-off satellite structures in the corresponding photoelectron spectrum. The multielectron processes due to the electron correlation are known to happen not only in the primary inner-shell hole creation processes but also in their relaxation processes. In the case of the shake-off transition, where two electrons are ejected simultaneously, the great intensity of the peaks in the zero electron kinetic-energy (ZEKE) spectrum arises through energy sharing between the two emitted electrons as their kinetic energy distribution is peaked with one electron having low kinetic energy electron and the other having correspondingly high kinetic energy. Thus, the ZEKE spectroscopy or threshold photoelectron spectroscopy (TPES) is very sensitive to this two-electron process, and is widely used for probing the multielectron processes in atoms and molecules.

The symmetries of the inner-shell excited states of small molecules can be deduced from the information obtained by the angle-resolved photoion spectroscopic (ARPIS) technique; the angularly resolved measurement of the fragment-ion emission with respect to the linear polarization of synchrotron radiation. The combination of ARPIS with TPES may provide additional information on the symmetries of the multielectron processes, such as multiply excited states and shake-up transitions in the core-ionization continua, which can be called "symmetry-resolved threshold photoelectron spectroscopy (SR-TPES or SR-ZEKES). In this report, we show that SR-TPES can be realized by a simple coincidence technique in which the coincident measurement between the threshold photoelectrons and angle resolved fragment-ions are employed. It is demonstrated that Σ– and Π–symmetries of the multiply excited states and correlation satellites in the K-shell ionization region of nitrogen are determined using this technique.

Experiments

The experiments were carried out on the bending magnet beamline BL4B at the UVSOR facility in IMS. The apparatus for SR-TPES is composed of an effusive gas source, a photoelectron energy analyzer specially designated for the efficient collection of low energy electrons, and two ion detectors. The threshold electrons extracted by a penetrating field through a lens system of the analyzer were focused onto the entrance slit and then energy- analyzed by a spherical sector electrostatic analyzer. The ion detectors on a plane perpendicular to the incident radiation were set at 0° and 90° relative to the electric vector of the light. The electron and ion signals were fed into a time-to-amplitude converter as start and stop signals, respectively. True coincidence signals produce a peak in a time-of-flight spectrum, while non-coincidence signals (random signals)

originating from the detection of two unrelated events yield a background in the spectrum. The SR-TPES spectra have been measured by scanning the photon energy with monitoring the intensity of the coincidence signals.

Results and discussion

The Π- and Σ-symmetry-resolved TPES spectra above the *K*-shell ionization threshold of N_2 are shown in Fig. 1 and 2, respectively, as compared to the conventional TPES spectra. Except for the very strong peak around 411 eV corresponding to the 1s threshold photoelectrons, two broad structures centered at 415 and 420 eV are dominant in the TPES spectrum. The higher energy band is know to be correspondent to some lower-lying N 1s shake-up satellites, assigned as the $1s^{-1}\pi^{-1}\pi^*$ configuration. The lower band can be assigned to the doubly excited states, on the basis of its energy position, which could decay through the channels producing low-energy electrons. The multiply excited states labeled C, D, E, and F, which have been identified in our previous APRIS work, may correspond to the features in the SR-TPES spectra. One can find that the peak C mainly consists of the Π-symmetry states, and the peak D is composed of the equivalent contributions from the Σ- and Π-symmetry states. The strong peak around 419 eV in the Σ-symmetry spectrum may be attributable to the shake-up satellite threshold with the $1s^{-1}\pi^{-1}\pi^*$ configuration having $^2\Sigma$ symmetry.

Further improvement on the data quality (statistics and energy resolution) of SR-TPES indicated in Fig.1 and Fig. 2 is obviously required for identifying all the spectral features related to the multielectron processes that are often buried in the strong single electron processes, which can be easily realized by performing the same experiments on an undulator based beamline. Fortunately a new undulator based beamline BL3U will be available in autumn 2003 and the present experimental method will be continuously developed on this beamline.

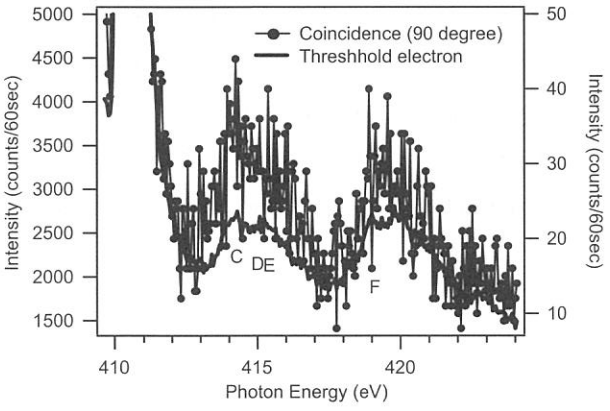

Fig. 1 The Π-symmetry-resolved threshold electron spectra of nitrogen

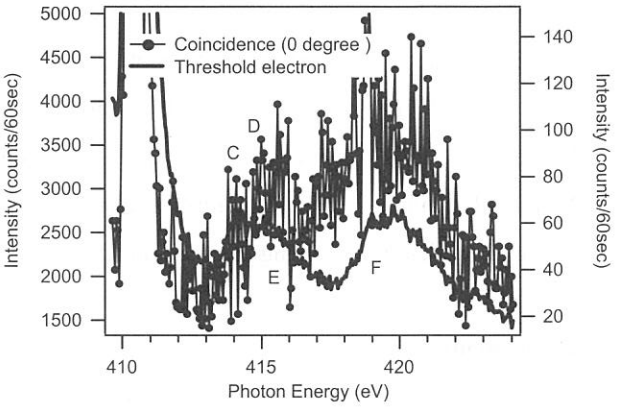

Fig.2 The Σ-symmetry-resolved threshold electron spectra of nitrogen

(BL4B)

Symmetry resolved photoabsorption spectra in the 2p excitation region of Cl_2

Eiji Shigemasa, Tatsuo Gejo, Takaki Hatsui, and Nobuhiro Kosugi

Institute for Molecular Science, Okazaki 444-8585, JAPAN

In order to identify the symmetries of molecular inner-shell excited states, polarization dependent studies have been widely applied to both chemisorbed and free molecules. The photodissociating molecules produced by a subsequent Auger decay of the inner-shell vacancy are not isotropically distributed in relation to the exciting radiation, because the absorption probability is greatest when the transition dipole moment is aligned with the electric vector of the incident radiation. Since the lifetime of the molecular inner-shell excited state is much shorter than the molecular rotation period, the angular distribution of the photofragments should show a corresponding anisotropy. For diatomic molecules, the measurements of the energetic fragment ions emitted parallel and perpendicular to the electric vector of the incident light achieve complete symmetry resolution between the $\Delta\Lambda=0$ (parallel) and $\Delta\Lambda=\pm1$ (perpendicular) transitions [1].

The 2p ionization spectra, or photoelectron spectra, show a molecular field splitting (MFS) and spin-orbit splitting (SOS). The 2p excitation spectra, or photoabsorption spectra, exhibit an exchange splitting (EXS) in addition to MFS and SOS. Due to the complexity in the theoretical treatments and the lack of the appropriate experiments, the assignments for the spectral features in the 2p excitation regions are not well established, even for simple diatomic molecules. We have already investigated very complicated spectral features due to EXS and SOS in the S 2p excitation region of SO_2, CS_2 and OCS [2], based on angle-resolved photoion spectroscopy (ARPIS) and the Breit-Pauli *ab initio* calculation. In the present work, Cl 2p ARPIS spectra of Cl_2 in comparison to HCl have been investigated. The lowest excited states in these molecules are the Cl 2p–σ^* excitation. There are three 2p orbitals, and the Cl 2p–σ^* excitation involves parallel and perpendicular transitions with respect to the bond direction.

The angle-resolved photoion measurements were performed on the beamline BL4B, equipped with a varied-line-spacing plane grating monochromator. Two identical ion detectors with retarding grids were used to detect energetic photoions (>5 eV) emitted at 0° and 90° with respect to the electric vector of the incident light. The $\Delta\Lambda=0$ component spectrum (I0) and $\Delta\Lambda=\pm1$ component spectrum (I90) were obtained by counting the signals from the 0° and 90° positioned detectors, as a function of the photon energy, respectively. The photon-energy resolution was set to about 50 meV for the present experiments.

The high-resolution Cl 2p ARPIS spectra of Cl_2 measured are displayed in Figure 1, in comparison to those obtained by the quantum chemical calculations. Concerning the

calculations for the Rydberg transitions, only lower Rydberg orbitals (4s, 5s, 4p and 3d) are taken into account. It is clear that the obtained I0 and I90 spectra nicely demonstrate the symmetry decomposition of the conventional photoabsorption spectrum. It is shown that theoretical ARPIS spectra for the σ* transition as well as lower-lying Rydberg states are reasonable agreement to the experimental data. The spectral profile for the σ* resonance in the experiments is quantitatively reproduced by the calculations. For the Rydberg transitions, the features are very complicated, but most features are rather well reproduced. It has also been found that the EXS effect can be neglected in the lower Rydberg states of Cl_2 considered in the present calculations, which is in sharp contrast to the 4s Rydberg state of HCl.

References
[1] E. Shigemasa et al., Phys. Rev. A 45, 2915 (1992).
[2] N. Kosugi et al., to be published.

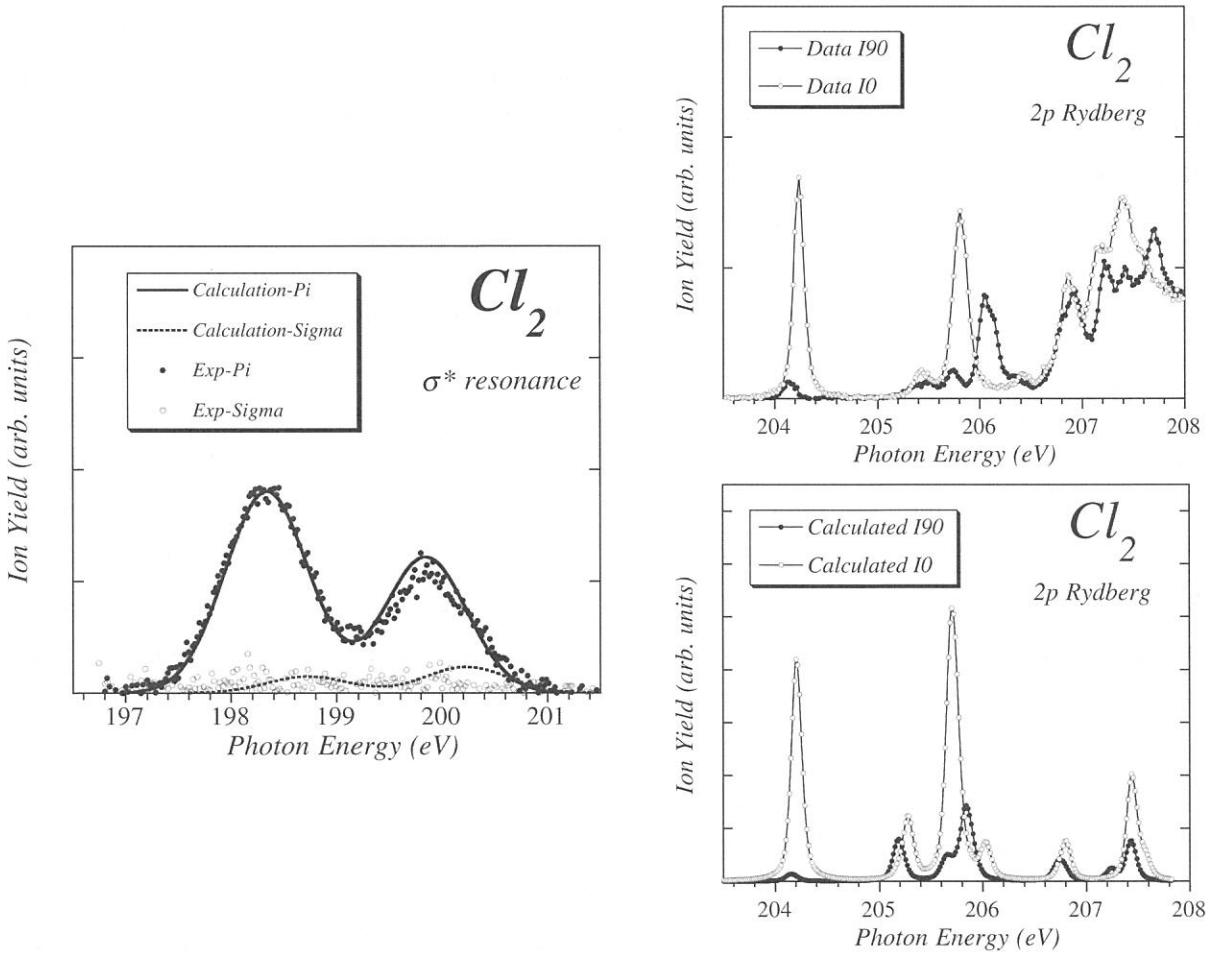

Fig. 1. High-resolution symmetry-resolved Cl 2p photoabsorption spectra of Cl_2.

(BL8B1)

Dissociation Processes of Core-excited CH_2F_2 in the C K-shell Excitation Region

H. Yoshida [a], K. Waki [a], Y. Senba [a], Y. Kawabe [a], T. Gejo [b], K. Mase [c], and A. Hiraya [a]

[a] *Department of Physical Science, Hiroshima University, Higashi-Hiroshima 739-8526, Japan*

[b] *UVSOR, Institute for Molecular Science, Okazaki, 444-8585, Japan*

[c] *Photon Factory, Institute of Materials Structure Science, Tukuba 305-0801, Japan*

Core-excited species are unstable and decay processes follow rapidly. The most dominant decay process is resonant Auger electron emission for light elements. In some case, nuclear motion is so fast that dissociation takes place on the same time scale (~fs) as Auger electron emission. Such dissociation in core-excited state is termed "ultra-fast dissociation". It was observed at first for HBr at the Br3d→ σ * excitation by detecting the atomic Auger emission from the core-excited fragment Br* [1]. The electronic decay from core-excited fragment was also observed for CH_2F_2, CHF_3, and CF_4 at the C1s→ σ * excitation [2]. Those were tentatively assigned to the electron emission from C* or CF*. To elucidate the detail of the ultra-fast dissociation processes for CH_2F_2, electron-ion coincidence measurements have been carried out at the soft x-ray beamline BL8B1.

The experimental procedure was described elsewhere [3]. Total ion yield spectrum for CH_2F_2 at the C1s excitation region is shown in Fig. 1. Some resonant structures, which were already assigned to σ *b_1, σ *a_1, and 3p [2], are observed in the spectrum. Fig. 2 shows the electron spectra following direct ionization of valence electron at hν = 286.1 eV (top), the C1s→ σ *b_1 resonant excitation at hν = 291.8 eV (middle), and the C1s→3p resonant excitation at hν = 294.1 eV (bottom). Horizontal axis indicates final-state energy (FSE) calculated by subtracting the electron energies from the initial excitation energies. By comparing these spectra, we notice that the intensity for the C1s→ σ *b_1 spectrum is fairly enhanced around 25 eV. This energy corresponds to the intermediate energy between participant Auger final states (10-20 eV) and spectator Auger final states (>30 eV). This structure was, thus, tentatively assigned to the electron emission from core-excited fragment [2]. Fig. 3 shows the coincidence spectra at FSE = 25 eV for the respective excitations described above. Horizontal axis indicates mass number. The spectrum for the C1s→3p (bottom) is quite similar to that for the valence ionization (top), while the spectrum for the C1s→ σ *b_1 (middle) is different from the others. A remarkable increase in the yield of CH_2^+ (m/q = 14) and a decrease in that of CH_2F^+ (m/q = 33) are recognized in the C1s→ σ *b_1 spectrum by comparing with the other two spectra. Such a considerable enhancement in the yield curve of CH_2^+ is observed only around 25 eV for the C1s→ σ *b_1. This implies that the emitting species are neither C* nor CF*. We suggest the following dissociation processes after the C1s→ σ *b_1 resonant excitation in CH_2F_2. At first, a C-F bond fission takes place in competition with Auger decay of a parent molecule in the core-excited states because of C-F anti-bonding character of σ *b_1 orbital. Then Auger decay from the core-excited fragment C^*H_2F produces an excited cation CH_2F^+* and it would dissociate effectively into CH_2^++F.

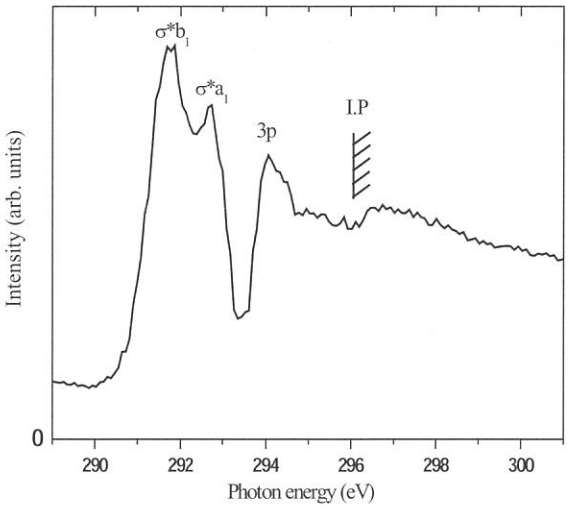

Fig.1 Total ion yield spectrum for CH_2F_2 at the C1s excitation region.

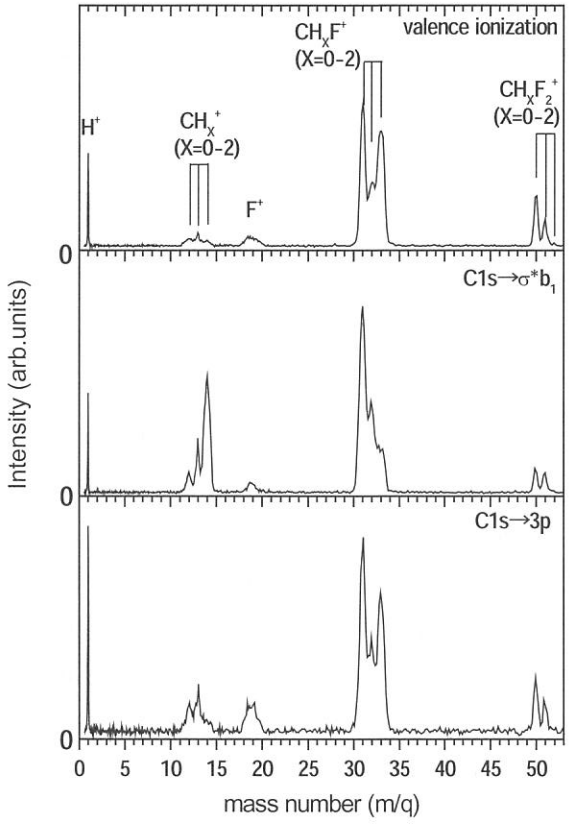

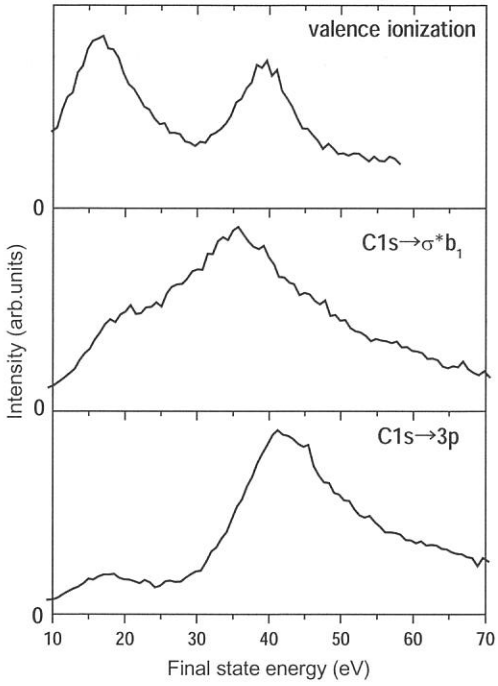

Fig. 2. Electron spectra following direct ionization of valence electron at hν = 286.1 eV (top), the C1s→ σ *b_1 resonant excitation at hν = 291.8 eV (middle), and the C1s→3p resonant excitation at hν = 294.1 eV (bottom).

Fig.3 Coincidence spectra at the FSE = 25 eV for direct ionization of valence electron at hν = 286.1 eV (top), the C1s → σ *b_1 resonant excitation at hν = 291.8 eV (middle), and the C1s→3p resonant excitation at hν = 294.1 eV (bottom).

References

[1] P. Morin and I. Nenner, Phys. Rev. Lett., 56 , 1913 (1986).

[2] K. Ueda et al., J. Electron Spectrosc. Relat. Phenom., 79 , 441 (1996).

[3] Y. Senba et al., to be published.